

# RSC Advances



This is an *Accepted Manuscript*, which has been through the Royal Society of Chemistry peer review process and has been accepted for publication.

*Accepted Manuscripts* are published online shortly after acceptance, before technical editing, formatting and proof reading. Using this free service, authors can make their results available to the community, in citable form, before we publish the edited article. This *Accepted Manuscript* will be replaced by the edited, formatted and paginated article as soon as this is available.

You can find more information about *Accepted Manuscripts* in the [Information for Authors](#).

Please note that technical editing may introduce minor changes to the text and/or graphics, which may alter content. The journal's standard [Terms & Conditions](#) and the [Ethical guidelines](#) still apply. In no event shall the Royal Society of Chemistry be held responsible for any errors or omissions in this *Accepted Manuscript* or any consequences arising from the use of any information it contains.

Cite this: DOI: 10.1039/c0xx00000x

www.rsc.org/xxxxxx

ARTICLE TYPE

# Use of CdTe Quantum Dots for High Temperature Thermal Sensing

Yangyang Li<sup>a</sup> and Ben Q Li<sup>\*b</sup>

Received (in XXX, XXX) Xth XXXXXXXXX 20XX, Accepted Xth XXXXXXXXX 20XX

DOI: 10.1039/b000000x

## 5 Abstract

An optical-thermal experimental system, in which CdTe quantum dots (QDs) were used as thermal sensors, is developed for micro-electromechanical systems (MEMS) temperature measurements in the high temperature range (> 70 °C). Laboratory-prepared CdTe QDs with properly controlled synthesis conditions show excellent temperature sensitivity. For orange emitting CdTe QDs, calibration from type A micro-heater yields a linear  
10 relation between the spectral peak shift and the temperature over the temperature range of 27 °C to 170 °C, the last being the highest temperature of the heater achieved in our current optical-thermal experimental setup. This linear relation is consistent with the predictions for semiconductor quantum systems from the principle of thermo-quantum mechanics for the temperature above the Debye point. Analysis of the experimental data indicates that the orange emitting QDs possess a thermally-induced spectral-shift sensitivity of 0.34 nm/°C, which is  
15 approximately about 2~3 times better than reported. The excellent repeatability and accuracy of the calibrated orange emitting CdTe QDs as thermal sensors are further demonstrated by applying them in monitoring electric thermal characteristic of type B MEMS structure. While calibration is for up to 170 °C, the temperature of up to 212 °C for type B MEMS heater was measured with a gratifying accuracy using the CdTe QDs, further demonstrating the stability of the thermal-spectral property of the QDs. The existence of a unique “burnout”  
20 spectrum in the temperature dependent PL spectra also suggests that optical-thermally sensitive QDs can be applied in both monitoring the temperature development and diagnosing circuit breakout due to over-heating.

## Introduction

Stimulated luminescence is light emitted by electronically  
25 excited quantum states that have been populated by an external optical radiation.<sup>1</sup> Among other factors, local temperature has a strong influence on the properties of the emitted photons. The relationship between the temperature and the stimulated luminescence properties may then be exploited to achieve thermal  
30 sensing of an object by the spatial and spectral analysis of the light emitted by the object. CdTe Quantum dots (QDs) are one of the widely studied quantum systems for medical imaging.<sup>2-5</sup> An important property of the QDs is that the spectral positions of the emission lines are distinctively determined by the energy  
35 separation between the two electronic levels, which are temperature dependent.<sup>6</sup> Thus the local thermal reading can be obtained by translating luminescence spectral shifts into temperature.

Several studies have appeared on the spectral shifts based  
40 temperature measurements applied to determine the temperature in nanoscale and biological cell systems. They provide an excellent means to map the temperature with a nanoscale spatial resolution.<sup>7-10</sup> The principle of the luminescence-based  
45 nanothermometry has been given in recent comprehensive reviews,<sup>11,12</sup> along with various applications involving nanoscale imaging and thermal measurements.<sup>13-19</sup> Of particular interest is the work by Li *et al.* who reported the use of single red colour

emitting CdSe QD to measure the temperature of a line-shape  
microstructure with a wavelength shift 0.093 nm/°C.<sup>13</sup> Also,  
50 reports have appeared on thermal sensitive fluorescence lifetime as a novel thermometry in micro and nano systems. Thermal image was obtained of a micro-fluidic chamber positioned between heating source by analyzing the spatial variation of the temperature sensitive luminescence lifetime of polymer that is  
55 introduced into the micro chamber.<sup>18</sup> Haro-González *et al.* examined how the CdTe QD luminescence lifetime varies within the biophysical thermal range (25~50 °C).<sup>19</sup> So far, much research has been focused on the use of the QDs thermal sensors for nanoscaled measurements, which are usually concerned with a  
60 low temperature range (25~50 °C). Little, if any, appears to have been explored for the use of these sensors for high temperature (> 70 °C) measurements. In light of a vast range of possible applications in science and engineering, such a study would open up an entirely different approach by which nanoscale thermal  
65 sensors are used for a macrosystem whose thermal behaviour cannot be determined by existing measurement techniques. For instance, these sensors may embedded in micro systems in diagnosis of microelectronic circuits and in determining thermal behaviour of ultra-high speed rotating object, such as high-speed  
70 rotating bearings, for which alternatives for thermal measurement are rather limited.

This paper presents a study on the use of CdTe QDs as thermal sensors to measure the temperature of and to monitor the thermal behaviour of micro/nano structured systems from room

temperature up to over 200 °C. The intention is to explore the effectiveness of these nanoscale thermal sensors, which has been proved useful for low temperature measurements, for high temperature applications. A key feature that differentiates the present study from those reported for thermal measurements using QDs is that a much higher spectral thermal sensitivity of 0.34nm/°C is obtained with the QDs synthesized in our own laboratory than those reported in literature. This improvement in sensitivity comes from proper control of synthesis conditions. Another distinct aspect of the present study is that this is perhaps the first work on the use of the nanothermal sensors for high temperature applications. In what follows, controlled synthesis of quantum dots designed for thermal sensing is discussed. Different colour emitting CdTe QDs have been successfully characterized and the thermal spectral characteristics of orange emitting QDs are well determined in a large-scaled temperature range. Use of them in non-contact, local temperature sensing of a MEMS heater is demonstrated. The experimental spectral data indicate us a novel technique which combines thermometry with on-line monitoring for micro/nano integrated circuits and fuse wires.

## Experimental

### Materials

Thioglycolic acid (TGA, 90%) and cadmium acetate ( $\text{Cd}(\text{CH}_3\text{COO})_2 \cdot 2\text{H}_2\text{O}$ , 99.5%) were purchased from Aladdin Chemistry. Sodium borohydride ( $\text{NaBH}_4$ , 96%) and potassium tellurite ( $\text{K}_2\text{TeO}_3$ , 99%) were supplied by Shanghai Zhenxin Chemical Reagents Factory. (Shanghai, China). All other reagents were of analytical grade and used directly without further purification.

### Synthesis of CdTe quantum dots

CdTe QDs were synthesized by modifying the method given in a previous paper.<sup>20</sup> In a typical synthesis, the molar ratio of  $\text{Cd}^{2+}/\text{TGA}/\text{TeO}_3^{2-}$  was 1.0: 1.0: 0.2, pH = 10.5~11.0. Briefly, 0.2 mM  $\text{Cd}(\text{CH}_3\text{COO})_2 \cdot 2\text{H}_2\text{O}$  was dissolved into 50 ml deionized water in a beaker. Then 18  $\mu\text{l}$  thioglycolic acid (TGA) was added and the pH was adjusted with 1M NaOH solution. After stirring for 5 min, 0.04 mM  $\text{K}_2\text{TeO}_3$  which was dissolved in deionized water was added into the above solution. Then 80 mg of  $\text{NaBH}_4$  was added into the precursor solution. After the reactions proceeded for another 5 minutes, all the solutions were transferred into a condenser and refluxed at 100 °C under open-air conditions. By this procedure, CdTe QDs with desired PL emission spectra can be obtained with different reaction times.

### Measuring system

Fig. 1 shows a schematic diagram of the experimental setup for temperature measurements. A mercury lamp is used as a light source. Ultraviolet wave band can be generated as the excitation light source through the fluorescence excitation module (attached to an inverted microscope, IX53, Olympus, Japan). Excitation light is directed through the microscope objective (40  $\times$ ) and focus onto the sample. The PL emission from QDs is collected by the same objective and directed through the fluorescence excitation module, channelled through a spectrograph (Shamrock SR-303i, Andor, British, grating 300 l/mm blazed at 500nm) for resolving the quantum dot emission spectra, and finally imaged

by an cool CCD camera (iDus DU420A-BV, Andor, British) with single FVB mode.

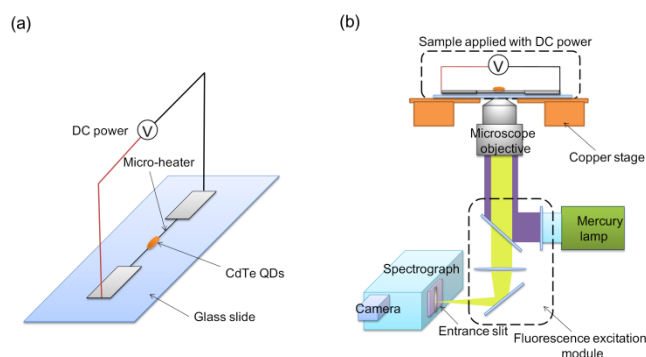


**Fig. 1** Experimental outline (a) Schematic diagram of CdTe QDs loaded micro-heater sample (b) Schematic of the experimental setup, illustrating the essential optical pathways in an inverted microscope.

### Preparation of MEMS micro-heater

The micro heater of aluminium film was fabricated on top of a Pyrex glass slide by a standard MEMS device fabrication process. The required micro fabrication facilities are available at the Institute for Advanced Manufacturing, Xi'an Jiaotong University. Briefly, the micro-heater patterns were realized by spin coating EPG533 photoresist on a clean glass slide. After a two-step soft bake (65 °C for 5 min and 95 °C for 10 min), the photoresist film was exposed to UV light for 12 s through a photo mask on which the desired microelectrode structure had been printed. Following another 10 min hard bake at 95 °C, the slide was gently vibrated in the developer solution for 20s to dissolve the exposed photoresist, leaving a negative relief containing the desired micro-heater patterns. Experimentally, we designed two different micro-heaters: type A with a line-shape structure while type B with a triangle-jointed shape in the middle of the structure. Afterwards, the aluminium film was realized by a magnetron sputtering system (Denton Vacuum explorer 14, USA). After finishing, the sputtering thickness of type A and type B micro-heater was 100 nm and 200 nm, respectively. The residual aluminium along with the unexposed photoresist was removed by a lift-off process. The specific dimensions are shown in Fig. 2a and b, the type A micro-heater is 1840  $\mu\text{m}$  long, 86  $\mu\text{m}$  wide and 100 nm thick while the type B micro-heater is 3780  $\mu\text{m}$  long, 86  $\mu\text{m}$  wide and 200 nm thick.

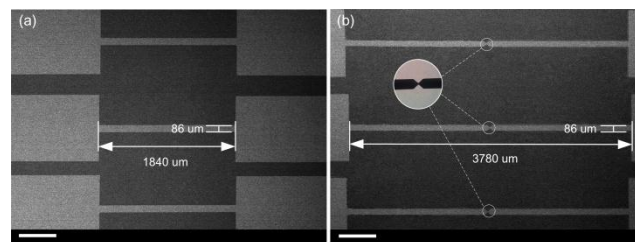


**Fig. 2** SEM photograph of type A and type B micro-heater. The inset scale bar is 500  $\mu\text{m}$ .

Conduit copper wires, through which DC power were supplied to the heater, were connected to the electrodes of

the micro heater using electrolongol, followed by a post bake at 80 °C for 30 min (Fig. S1†). This ensured good contact between the electrodes and the copper wires.

### Quantum dots as thermal sensors

Orange emitting QDs were added every three micro-heater among the MEMS heater arrays (Orange QDs were chosen here for convenience; other QDs are equally qualified for the same study). Specifically, 10  $\mu$ L of 0.2 mM CdTe quantum dots (QDs) solution were dropped in the middle of type A and type B micro-heaters with a post bake at 100 °C in vacuum to evaporate surplus solvents. Both the copper wire connection and quantum dots deposition processes were carried out under a home-built microscopic probe station.

### Temperature calibration and measurement

The temperature of a MEMS micro-heater was controlled to change by tuning the potential between the electrodes. The whole system is placed in the measuring section as shown in Fig. 1b. The excitation light for QDs from the mercury lamp was focused on the middle area of micro-heater by adjusting the location of the sample. The light emitted by the QDs passed the microscope, and was magnified 40 $\times$  and focused by the micro objective. This produced a light image of the QDs, which was dispersed by the spectrograph. The spectrum of the emitted light was detected and analyzed by the CCD camera. As a temperature change caused a corresponding spectrum peak shift, the temperature of a sample can be measured by measuring the peak shift. For the temperature above the Debye point, the spectral peak shift is linearly correlated to the temperature. Thus, knowing the value of the peak shifts of the light emitted by QDs allows the temperature of the sample to be determined. For the present study, the type A micro-heater was used to calibrate the QDs thermal sensor, while the type B micro heater was used as a demonstration of QDs as high temperature thermal sensor.

## Results and Discussion

### Quantum dots synthesis

Water soluble QDs were synthesized as described in previous section following the scheme as shown in Fig. 3a. Once the formation of CdTe nanocrystal core was completed, the growth of the CdTe QDs during the refluxing was controlled by the Ostwald ripening process, in which smaller particles dissolve and the monomers released are consumed by larger ones.<sup>21,22</sup> This stems from the fact that molecules on the surface of a particle are energetically less stable than the ones in the interior. To specifically put it, large particles are more energetically favourable since more atoms are bonded to the neighbours and fewer atoms are at the unfavourable surface. As the system tries to lower its overall energy, molecules on the surface of a small particle will tend to detach from the particle and diffuse into the solution. When all small particles do this, it increases the concentration of free atoms in solution. When the free atoms in solution are supersaturated, the free atoms have a tendency to condense on the surface of larger particles. Therefore, all smaller particles shrink, while larger particles grow, and overall the average size will increase as in Fig. 3a.

The TGA-stabilized CdTe QDs aqueous solutions were taken from the refluxing reaction mixture at different intervals of time. The images of the TGA-coated CdTe QDs irradiated under an ultraviolet lamp were recorded. A typical set of these images is given in Fig. 3b, where the colour of the CdTe QDs was made to turn from green to yellow, orange and dark red by controlling the reflux reaction times. It is noted that poor PL intensity was obtained at the initial nucleation stage, due to the existence of surface defects of the QDs that contributed to nonradiative recombination as in Fig. 3c. As the reaction went on, a partial hydrolysis of TGA occurred in the course of refluxing and the incorporation of sulfur into the CdTe nanocrystals formed a thin CdS molecular layer. A large amount of surface traps of CdTe nanocrystals were effectively eliminated due to formation of a CdS layer, leading to a tremendous enhancement in PL intensity as in Fig. 3d. The PL intensity reached the maximum value in the case in which the thickness of CdS layer increased to a critical threshold (the optimum thickness). Afterward, the PL intensity declined while continuing to prolong the reaction time. The reason was that dislocations and new defects formed as the thickness of the CdS molecular layer increased unceasingly, which resulted from the intrinsic interfacial strains due to the lattice mismatch (10.0 %) between CdTe and CdS as in Fig. 3e.<sup>23</sup> These defects may become a new source of nonradiative recombination sites and cause a decrease in the PL intensity of CdTe QDs.<sup>24</sup>

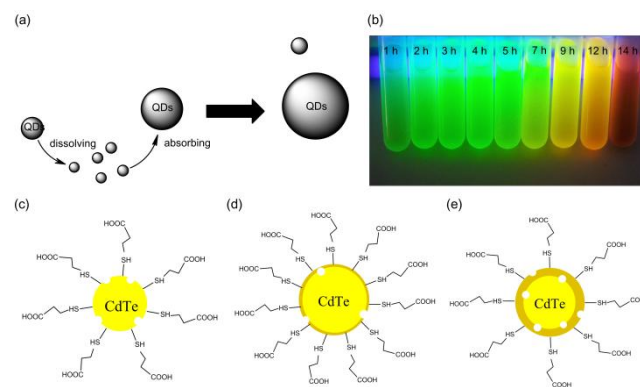


**Fig. 3** Schematic of CdTe QDs formation (a) and photoluminescence photograph of CdTe QDs solution (b) taken at 1h, 2h, 3h, 4h, 5h, 7h, 9h, 12h and 14h in sequence (from left to right). Initial surface defects in bare CdTe QDs (c), surface-improved CdTe QDs with a thin CdS molecule layer (d), interfacial strain induced defects in CdTe QDs with a thick CdS shell (e). White circles represent defects mentioned above.

Commonly, quantum dots with fewer defects exhibit higher PL quantum yields and better spectral characteristics, which is favourable for the optothermal experiment. According to previous work, QDs whose emission ranged from 520 nm to 600 nm obtained relative higher PL quantum yields and stable optical properties, to a great extent, reducing the influence of defects.<sup>20</sup> Thus, CdTe QDs synthesized at 4h, 9h and 12h intervals of time (called green, yellow and orange emitting QDs, respectively) were chosen as our experimental subject.

### Characterization of CdTe quantum dots

The CdTe QDs obtained above were characterized by a transmission electron microscope (TEM, JEOL-2100) operated at

200 kV. The UV/Vis absorption was measured by a spectrophotometer (Shimadzu 3100PC UV-Vis-NIR spectrophotometer). The PL spectra were dispersed by a spectrograph (Shamrock SR-303i, grating 300 l/mm blazed at 500nm, Andor, British) with a subsequent imaging by a cool CCD camera (iDus DU420A-BV, Andor, British).

Fig. 4 compares the characteristics of three different CdTe QDs refluxing at a reaction of 4h, 9h and 12h (the TEM image (Fig. 4a), UV/Vis absorption spectra (Fig. 4b) and PL emission (Fig. 4c). Nanometre features of green, yellow and orange emitting CdTe QDs have been further confirmed by the clear lattice fringes in the TEM images, from which the size of each colour emitting quantum dot was about 2.34 nm (green), 2.78 nm (yellow) and 2.95 nm (orange), respectively. The measurements also indicate that the absorption spectra and the PL emission spectra both experience a red shift (that is, the peak shifts to a longer wavelength) with an increase in the size of the CdTe QDs. Specifically, the green, yellow and orange emitting CdTe QDs have a corresponding peak wavelength of 487 nm, 505 nm and 515 nm in absorption spectra and of 550 nm, 570 nm and 590 nm in the PL emission. This effect of the quantum confinement is consistent with the size effect predicted by the first order perturbation analysis from quantum mechanics.<sup>25</sup>

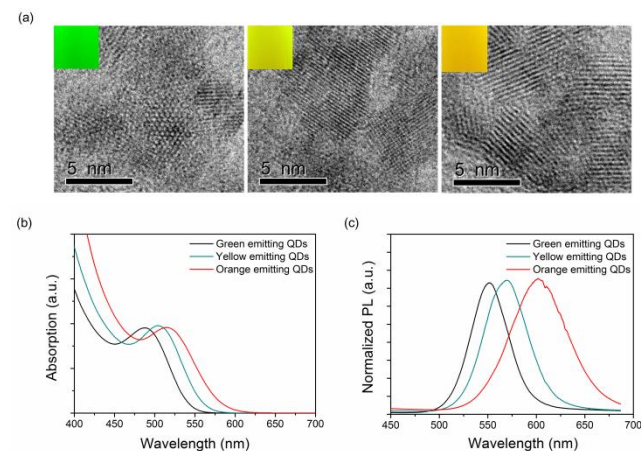


**Fig. 4** CdTe quantum dots characterization. (a) Highly magnified TEM and photograph of the photoluminescence from green, yellow and orange emitting CdTe QDs. (b) Absorption spectra and (c) Photoluminescence spectra of green, yellow and orange emitting CdTe QDs show stable luminescence under UV lamp with centre excitation wavelength 365 nm.

### Temperature calibration with type A micro-heater

While other colour-emitting QDs are equally useful, the orange-emitting CdTe QDs were used as thermal sensors for high temperature monitoring. To provide needed thermal information, the PL spectra of the orange-emitting CdTe QDs were calibrated with type A micro-heater. The 300 l/mm grating of spectrograph (*i.e.* the system in Fig. 1b) was used to disperse the filtered emission with a CCD exposure time of 1.5 s at each thermal equilibrium point. The equilibrium temperature of the micro-heater was regulated by controlling the different voltages supplied to, and was measured by the thermocouple attached to, the heater. Thermocouple hot end was placed in the middle of line-shaped type A heater (Fig. S2a†). The temperatures and the corresponding PL emission spectra are shown in Fig. 5c as a

function of the applied voltages. The calibration tests for the orange emitting QDs were done twice to ensure good repeatability (orange emitting QDs I, II). In each case, the spectral data and thermal couple indications were obtained with a voltage interval of 0.5 V from 0 V to 6.5 V and 6 V under an equilibrium electrothermal condition. The spectrum detecting process was continued until the micro resistance wires were fused.

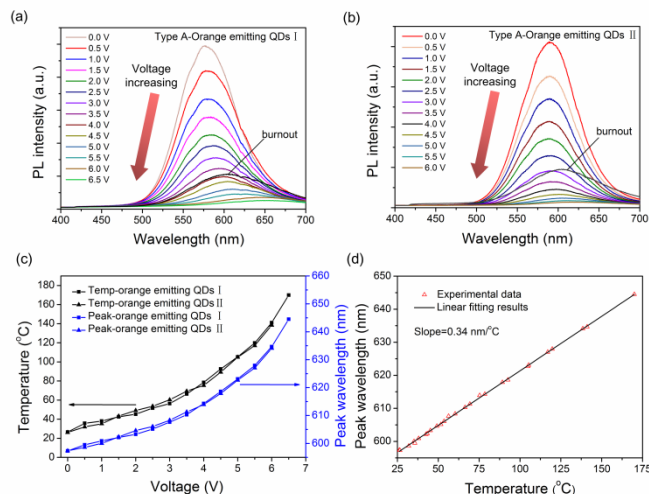


**Fig. 5** (a) and (b) PL emission spectra for orange emitting QDs under different electrode potentials for type A micro-heater. (c) Temperature and peak wavelength changed with applied electrode potentials. Insert is the photograph of MEMS temperature measurement using thermocouple. (d) Wavelength shift as a linear function of temperature.

From Fig. 5a, b and c, it is seen that the peak wavelength of CdTe QDs exhibits a red shift almost quadratically as the applied voltages increases and so does the temperature rise registered by the thermocouple. The average emission intensity is also shown decreased with a broadening in spectral width. Both wavelength shift and emission intensity decline were reversible during the experiments performed. From quantum-thermal theory of semiconductors,<sup>26,27</sup> an increase in temperature changes the dilation energy of a quantum system (in this case, quantum dot), which leads to a change in energy bandgap. More specifically, intratomic spacing dilates when the amplitude of the atomic vibrations is enlarged as a result of the applied thermal energy. An increased interatomic spacing decreases the potential seen by the electrons. Consequently, the energy bandgap is reduced. As the energy band is closely related to the light frequency, the wavelength of light emitted by a quantum system changes with the temperature of the system. This provides the basis for temperature measurements. Studies further show that at the temperature of above critical point, the shift in the wavelength of light emitted by a quantum system is correlated linearly with the temperature.<sup>28,29</sup> In terms of the decreased emission intensity, it is believed that CdTe core is not capped with a thicker CdS shell and the thinner shell lets the core regions on surface of nanocrystal expose to the environment, so that the increased temperature disturbs the repopulation of mobile electrons and holes on the surface of water soluble QDs.<sup>30</sup> Therefore, some reactions such as oxidation would occur and most carriers that were in deep trap sites emit nonradiatively, which cause the decrease of PL intensity of water soluble CdTe QDs.<sup>31</sup>

Analytically, all the initial spectra under different potentials were disposed with Gaussian fits. Wavelengths extracted from processed results were done with a further linear fitting (fitting adjustment factor  $R^2 = 0.99948$ ) versus temperature (Fig. 6d).

$$\text{Wave}_{p\text{-orange}} = 588.35 + S_{\text{orange}} * T_{\text{orange}} \quad (1)$$

The linear fitting equation for orange emitting QDs spectra was presented as equation (1) with a slope value  $S_{\text{orange}} = 0.33006 \text{ nm}/^\circ\text{C}$ , in which  $\text{Wave}_{p\text{-orange}}$  represent spectral peak wavelength of orange emitting CdTe QDs under a local temperature  $T_{\text{orange}}$ . The slope of the fitting curves intuitively reflects the temperature sensitivity of wavelength shift for CdTe QDs.

The accuracy of the CdTe QDs as an optical thermal probe is influenced by two factors: the accuracy of the wavelength shift ( $\delta = 0.04 \text{ nm}$ ) measured by the spectrograph and the standard deviation error ( $\sigma_{\text{orange}} = 0.0015 \text{ nm}/^\circ\text{C}$ ) of the spectral linear fitting procedures. The wavelength accuracy ( $\delta$ ) depends on the spectrograph itself, only such a small value can lead to a deviation from the exact temperature. This deviation is determined by  $e_{T\text{-orange}} = (\delta) / (S_{\text{orange}} \pm \sigma_{\text{orange}})$  with a final value  $0.12 \text{ }^\circ\text{C}$ . Another indicator in micro/nano scale thermometry we care about is the temperature resolution  $\Delta T$ , which is directly determined by the spectral resolution ( $\Delta\lambda = 0.13 \text{ nm}$ ) of the experimental configuration. The highest thermal resolution of the orange emitting CdTe QDs-based thermal probe is expected to be close to  $0.39 \text{ }^\circ\text{C}$  by  $\Delta T = \Delta\lambda / S_{\text{orange}}$ . According to temperature-dependent energy band theory, can be extended to a broader temperature range from  $27 \text{ }^\circ\text{C}$  to  $500 \text{ }^\circ\text{C}$ .<sup>32</sup>

As seen in Fig. 6a and b, the “burnout” voltage differed from each group, with a minimal value 6 V and maximal value 6.5 V. PL emission spectra of CdTe QDs became more flat with incremental applied voltages. This phenomenon is due to a large accumulation of Joule heat with an increasing external potential. Noticeably, the moment micro-heater fused, inverse changes in PL emission spectra occurred as a result of the sudden disappear of heat source (the black curve labelled “burnout” in Fig. 6a and b). Though the “burnout” spectra PL intensities were far lower than initial emission spectra, there was an apparent PL enhancement in “burnout” spectra compared with “close to fusing” emission spectra (close to abscissa axis). All these ensemble temperature-dependent spectroscopic characteristics appeared to be reproducible.

### High temperature measurement with quantum dots

To demonstrate the CdTe QDs as a useful thermal sensor for high temperature applications, the orange emitting CdTe QDs, whose photospectrothermal behaviour was calibrated using type A micro heater above, were used to measure the unknown temperature of type B micro-heater. For this purpose, the CdTe QDs were placed at the triangularly shaped joint at the middle of the type B MEMS heater. To validate the measurements by the QDs, a thermocouple (5SC-TT-K-45-36; Omega Engineering, Inc.) is attached to the heater just at the triangle-jointed point (Fig. S2b†). This was done under a microscopic probe station. The PL emission spectra of the CdTe QDs were acquired by the system shown in Fig. 1b for the voltage range of 0 V to 9 V with a 1 V interval. Spectral results are shown in Fig. 6a and b, where the thermophotspectral phenomena, similar to Fig. 5a and b, are observed with increasing electrode potentials, and the “burnout”

spectra are evident when the type B MEMS heater was fused at a maximal voltage of 9V.

It is important to note that the “burnout” spectrum curve distinguishes itself from the rest of CdTe QDs thermophotspectra and thus this unique characteristic may serve as a useful on-line monitoring method to detect the born-out-induced malfunction of micro/nano integrated circuit.

The PL spectra of CdTe QDs changed reversely as temperature reverses, but initial emission peak and intensity position was never to be reached, as we can see the “burn out” curves in Fig. 5a, b and Fig. 6a, b. This phenomenon was due to the thermal induced surface trap states and oxidative damages which depressed the restoration of the CdTe lattice thermal expansion and impeded the recovery process of PL spectra.

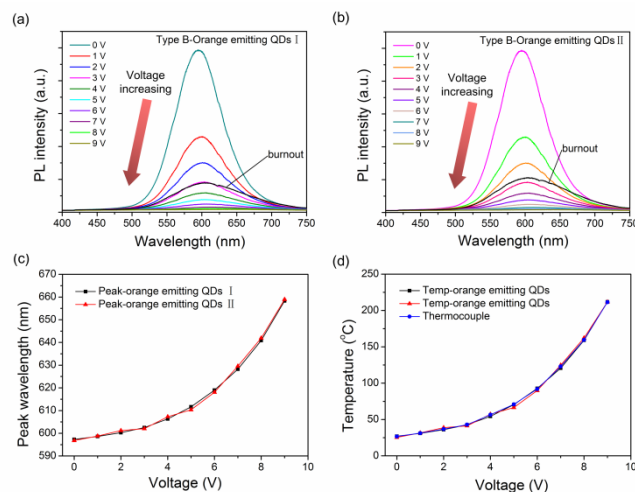


**Fig. 6** (a) and (b) PL emission spectra for orange emitting QDs under different electrode potentials for type B micro-heater.(c) Orange emitting QDs peak wavelength changed with applied voltages. (d) Micro-heater temperature as a function of electrode potentials. Insert is the photograph of MEMS temperature measurement using thermocouple.

Fig. 6 illustrates the measured characteristics of the orange-emitting QDs (I, II). The repeatability is excellent as indicated by the spectral curves in Fig. 6a, b and by the peak positions of the thermophotspectra in Fig. 6c. The temperature readings by the QDs shown in Fig. 6d were obtained by substituting the values of the spectral peak positions into the calibration relation given by Eq. (1). The readings are plotted along with those registered by the thermocouple. Clearly, the temperatures at the centre of the micro-heater versus applied voltages also manifested an approximately quadratic relationship up to a maximal value of  $212 \text{ }^\circ\text{C}$ , which is expected as the Joule heating is proportional to the square of the applied voltage (or current).<sup>33</sup> A reasonably good accuracy of QDs as a thermal sensor is validated by the fact that the two curves of the thermocouple and the QDs essentially duplicate each other. Detailed analysis of the collected data indicates a temperature deviation of  $0.3 \text{ }^\circ\text{C}$  between the quantum dots measurements and the thermocouple reading. Inspection of the results in Fig. 6c and d confirms the stability and repeatability of CdTe QDs as thermal sensors for non-contact optical temperature measurement. Finally, it is worth pointing out that while the thermophotspectral calibration is performed only for up to  $170 \text{ }^\circ\text{C}$ , because of the thermal capacity limit of the type A

micro heater, the extended use of this calibration up to 212 °C appears fully justified by the data shown in Fig. 6. This provides additional support data for the linear thermophotospectral relation predicted by the principles of thermoelastics and quantum mechanics for quantum systems at high temperatures (that is, above the Debye temperature).

Studies show that the electrothermal characteristics of a MEMS device can be affected by various factors, including the dimensions, thermal properties, input current, instrument parameters and surroundings.<sup>34</sup> The background noise of the spectrum detector (such as dark current in device) may influence the accuracy of determining the spectral peak position, though it can be minimized by improving exposure time.

Numerical simulation for both type A and B micro-heaters thermoelectric coupling suggested us a maximal heat accumulation in the middle of the structure. Excessive Joule heating causes the fusing of the structure, which is confirmed by our experiment. The “burnout” spectra, compared to “close to fusing” spectra, have an obvious PL enhancement (shown in Fig. 5a, b and Fig. 6a, b) due to the sudden disappear of electrothermal heat source. This spectral jump can be used as a trigger signal to raise the alarm, serving as on-line dynamic monitoring for key position of micro/nano integrated circuit and fuze wires. From this point, our method will be a combination of thermometry and dynamic monitoring.

While proved by the present work, the usefulness of this luminescence-based, reversible and linear change in PL wavelength shift of the CdTe QDs over a wide temperature range near ambient conditions establish their utility as optical temperature indicators for a variety of applications, e.g., CdTe QDs embedded in some polymer thin films may be used as temperature-sensitive coatings in contactless monitoring of ball bearing temperature by fixing them on the end face of inner and outer raceway or the surface of the bearing cage. Other jobs have shown that individual QDs possess equally well temperature sensitivity compared with the ensemble of QDs. In a biosystem, single CdTe QD coated with biocompatible molecules could be taken into living cell by endocytosis. When lesion occurs in living cell or surrounding changes, small temperature variations (no more than several Celsius) will be reflected on the luminescent spectroscopy.

## Conclusion

This paper has reported an optical-thermal experimental system for temperature measurements in which CdTe QDs are used as thermal sensors. Thermally sensitive CdTe QDs with different sizes were synthesized under properly controlled conditions and characterized under room temperature. The orange emitting CdTe QDs were calibrated with type A micro-heater, giving a linear relation for the temperature and the spectral peak shifts over the temperature range of 27 °C to 170 °C, the highest temperature of the heater achieved in our current optical-thermal experimental setup. This result is consistent with the linear relation predicted theoretically for semiconductor QDs from the principle of thermo-quantum mechanics for the temperature above the Debye point. Results show that the orange emitting QDs possess a thermally-induced spectral-shift sensitivity of 0.34 nm/°C, which is approximately about 2~3 times better than

reported. Calibrated with type A heater, orange emitting CdTe QDs were used in monitoring electric thermal characteristic of type B MEMS structure, acquiring satisfactory repeatability and accuracy. This further demonstrates the usefulness of QDs as excellent thermal sensors. While calibration was for up to 170 °C, CdTe QDs were used as thermal sensors with good accuracy up to the temperature of 212 °C for type B MEMS heater. The good accuracy and repeatability in extending beyond the calibration range suggests a very stability of the temperature-spectral property of the CdTe QDs. The existence of a unique “burnout” spectrum in the temperature dependent PL spectra also suggests that QDs may also be useful in diagnosing a circuit malfunction due to over-heating.

## Acknowledgements

The authors are grateful to the International Research Centre for Dielectric for TEM characterization; Micro-nano Manufacturing Centre for MEMS structure fabrication; Dr. Wei Yu and Xinbing Jiang for useful comments and general discussion on the paper.

## Notes and references

<sup>a</sup>State Key Laboratory for Manufacturing Systems Engineering, School of Mechanical Engineering, Xi'an Jiaotong University, 710049 Xi'an, China. E-mail: liyang617730@stu.xjtu.edu.cn

<sup>b</sup>Department of Mechanical Engineering, College of Engineering and Computer Science, University of Michigan-Dearborn, MI 48128, USA. FAX: 1-313-593-3851; Tel: 1-313-593-5241; E-mail: benqli@umich.edu

† Electronic Supplementary Information (ESI) available: Fig. S1-2. See DOI: 10.1039/b000000x/

- 1 H. C. Ishikawa-Ankerhold, R. Ankerhold and G. P. C. Drummen, *Molecules*, 2012, **17**, 4047-4132.
- 2 M. Dahan, T. Laurence, F. Pinaud, D. S. Chemla, A. P. Alivisatos, M. Sauer and S. Weiss, *Opt. Lett.*, 2001, **26**, 825-827.
- 3 A. P. Alivisatos, W. Gu and C. Larabell, *Annu. Rev. Biomed. Eng.*, 2005, **7**, 55-76.
- 4 V. Biju, T. Itoh, A. Anas, A. Sujith and M. Ishikawa, *Anal. Bioanal. Chem.*, 2008, **391**, 2469-2495.
- 5 G. P. C. Drummen, *International Journal of Molecular Sciences*, 2010, **11**, 154-163.
- 6 R. Pässler, *J. Appl. Phys.*, 2001, **89**, 6235.
- 7 L. M. Maestro, E. M. Rodríguez, F. S. Rodríguez, M. C. I. la Cruz, A. Juarranz, R. Naccache, F. Vetrone, D. Jaque, J. A. Capobianco and J. G. Solé, *Nano Lett.*, 2010, **10**, 5109-5115.
- 8 L. M. Maestro, C. Jacinto, U. R. Silva, F. Vetrone, J. A. Capobianco, D. Jaque and J. G. Solé, *Small*, 2011, **7**, 1774-1778.
- 9 J. M. Yang, H. Yang and L. Lin, *ACS Nano*, 2011, **5**, 5067-5071.
- 10 G. Kucsko, P. C. Maurer, N. Y. Yao, M. Kubo, H. J. Noh, P. K. Lo, H. Park and M. D. Lukin, *Nature*, 2013, **500**, 54-58.
- 11 D. Jaque and F. Vetrone, *Nanoscale*, 2012, **4**, 4301-4326.
- 12 C. D. S. Brites, P. P. Lima, N. J. O. Silva, A. Millán, V. S. Amaral, F. Palacio and L. D. Carlos, *Nanoscale*, 2012, **4**, 4799-4829.
- 13 S. Li, K. Zhang, J. M. Yang, L. W. Lin and H. Yang, *Nano Lett.*, 2007, **7**, 3102-3105.
- 14 R. S. Yang, L. W. Chang, J. P. Wu, M. H. Tsai, H. J. Wang, Y. C. Kuo, T. K. Yeh, C. S. Yang and P. Lin, *Environ. Health Persp.*, 2007, **115**, 1339-1343.
- 15 W. J. Parak, T. Pellegrino and C. Plank, *Nanotechnology*, 2005, **16**, 9-25.
- 16 D. R. Larson, W. R. Zipfel, R. M. Williams, S. W. Clark, M. P. Bruchez, F. W. Wise and W. W. Webb, *Science*, 2003, **300**, 1434-1436.
- 17 L. M. Maestro, J. E. Ramírez-Hernández, N. Bogdan, J. A.

- Capobianco, F. Vetrone, J. Solé-García and D. Jaque, *Nanoscale*, 2011, **4**, 298-302.
- 18 E. M. Graham, K. Iwai, S. Uchiyama, A. P. de Silva, S. W. Magennis and A. C. Jones, *Lab Chip*, 2010, **10**, 1267.
- 5 19 P. Haro-González, L. Martínez-Maestro, I. R. Martín, J. García-Solé and D. Jaque, *Small*, 2012, **8**, 2652-2658.
- 20 S. L. Wu, J. Dou, J. Zhang and S. F. Zhang, *J. Mater. Chem.*, 2012, **22**, 14573-14578.
- 21 V. Swayambunathan, D. Hayes, K. H. Schmidt, Y. X. Liao and D. Meisel, *J. Am. Chem. Soc.*, 1990, **112**, 3831-3836.
- 10 22 S. Lee, I. Daruka, C. S. Kim, A. L. Barabási, J. L. Merz and J. K. Furdyna, *Phys. Rev. Lett.*, 1998, **81**, 3479-3482.
- 23 Y. He, H. T. Lu, L. M. Sai, Y. Y. Su, M. Hu, C. H. Fan, W. Huang and L. H. Wang, *Adv. Mater.*, 2008, **20**, 3416-3421.
- 15 24 Y. He, H. T. Lu, L. M. Sai, W. Y. Lai, Q. L. Fan, L. H. Wang and W. Huang, *J. Phys. Chem. B*, 2006, **110**, 13370-13374.
- 25 L. Brus, *The Journal of Physical Chemistry*, 1986, **90**, 2555-2560.
- 26 H. Y. Fan, W. Spitzer and R. J. Collins, *Physical Review*, 1956, **101**, 566-572.
- 20 27 J. Bardeen and W. Shockley, *Physical Review*, 1950, **80**, 72-80.
- 28 Y. P. Varshni, *Physica*, 1967, **34**, 149-154.
- 29 K. P. O'Donnell and X. Chen, *Appl. Phys. Lett.*, 1991, **75**, 2924-2926.
- 30 T. C. Liu, Z. L. Huang, H. Q. Wang, J. H. Wang, X. Q. Li, Y. D. Zhao and Q. M. Luo, *Anal. Chim. Acta*, 2006, **559**, 120-123.
- 25 31 A. Eychmüller, A. Hässelbarth, L. Katsikas and H. Weller, *Ber. Bunsen. Phys. Chem.*, 1991, **95**, 79-84.
- 32 C. Allahverdi and M. H. Yükselici, *New J. Phys.*, 2008, **10**, 103029.
- 33 B. Q. Li, *Int. J. Eng. Sci.*, 1993, **31**, 201-220.
- 34 L. W. Lin and M. Chiao, *Sens. Actuators, A*, 1996, **55**, 35-41.

30